Shock Waves (1997) 7: 275–285

Shock Waves

Shock wave interaction with a cloud of particles

V.M. Boiko, V.P. Kiselev, S.P. Kiselev, A.N. Papyrin, S.V. Poplavsky, V.M. Fomin

Institute of Theoretical and Applied Mechanics, Russian Academy of Sciences, Novosibirsk 630090, Russia

Received 15 April 1996 / Accepted 3 June 1996

Abstract. The present paper is devoted to experimental and theoretical investigation of the shock wave (SW) propagation in a mixture of gas and solid particles in the presence of explicit boundaries of the two-phase region (cloud of particles). The effect of the qualitative change in the supersonic flow behind the SW in a cloud of particles within the range of the volume concentration of the disperse phase 0.1-3% is experimentally shown and theoretically grounded.

Key words: Shock wave interaction, Cloud particles, Computational simulation, Laser visualization

Nomenclature

C_d: drag coefficient of a particle
d, r_s: diameter, radius of a particle
D: velocity of the cloud center of mass
f: distribution function
m: volume concentration
n: number density of particles
v, w: velocity components in x and y directions
ρ: density
p: pressure
T: temperature
E: specific internal energy
γ: specific heat ratio
μ, λ: viscosity and heat conductivity coefficients
c_v, c_s: heat capacities of gas and particles
τ: time of particle velocity relaxation
τ_v: time of gas velocity relaxation
Kn, Re, Nu, Pr: Knudsen, Reynolds, Nusselt and Prandtl numbers
M_0: shock wave Mach number
M_1: gas flow Mach number
M_{12}: Mach number of the relative motion of gas and particles

subscripts
1: gas parameters
2: particle parameters

Correspondence to: V.M. Fomin

1 Introduction

In a number of technological processes of powder production and processing one should take care about a dust explosion. An important reason for this is a shock wave propagating the dusty gas mixture. Detailed knowledge of the relaxation processes behind the SW front at temperatures and pressures typical for dusty gas explosions are required for physical and mathematical simulation of this phenomenon. In particular, one of the fundamental problems is the velocity relaxation of the phases in the flow behind the SW front (Ivandaev et al. 1981; Soo 1971).

The major part of experimental efforts in this field covers subsonic flows. The velocity nonequilibrium in supersonic flows is scantily explored where the relative Mach number of gas and particles varies within a wide range during the velocity relaxation process. Vast experimental data on C_d for a single particle are presented in (Bailey and Hiatt 1972; Bailey and Starr 1976). A large number of correlational dependences $C_d = C_d(M, Re)$ is also available in (Bailey and Hiatt 1972; Bailey and Starr 1976; Carlson and Hoglund 1964; Henderson 1976; Rudinger 1970; Selberg and Nicholls 1968). However, in the flows with high concentration of the disperse phase the value of C_d deviates considerably from the values typical of single particles. Thus, in low-velocity two-phase flows this effect becomes noticeable in fairly concentrated mixtures $m_2 \geq 5\%$ (Gorbis 1964) while in a supersonic nozzle these effects are manifested already at $m_2 \geq 1\%$ (Yanenko et al. 1980).

The lack of knowledge on two-phase flows (on the peculiarities of the gas phase behavior, in particular) behind the SW in a cloud of particles calls for further research in this direction. Nevertheless, since no experimental methods for measuring the gas parameters in nonequilibrium two-phase flows are available, mathematical simulation of the process of the SW/cloud interaction becomes urgent. Therefore, the present paper suggests two approaches to the problem:

- experimental investigation of the physical mechanisms of the SW/cloud interaction;

- mathematical simulation of the SW propagation in a cloud of particles.

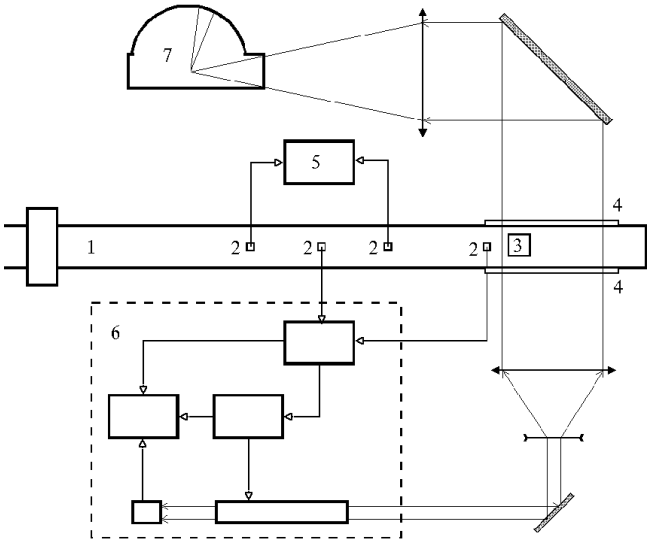

Fig. 1. Layout of experimental facility. 1 - shock tube, 2 - pressure transducers, 3 - device introducing particles, 4 - windows, 5 - time intervals sensor, 6 - laser stroboscope, 7 - high-speed photocamera

2 Experimental investigation of the physical mechanisms of the SW/cloud interaction

2.1 Experimental facility

The experiments were carried out in a shock tube equipped with devices for the optical visualization of the shock wave processes in two-phase media, for measuring the pressure profiles and the shock wave velocity (Fig. 1). Driver and driven sections were 1.5 and 5 m long, respectively; the channel cross section was $52 \times 52\,\mathrm{mm}^2$. The pressure of the driver gas (helium) and the driven gas (air) were, respectively, $2.5 - 10$ MPa and $0.01 - 0.1$ MPa. The SW Mach range was $M_0 = 1.5 - 4.5$. The gas parameters behind the SW were determined through the measured Mach number M_0 taking into account the temperature dependence of the specific heat ratio (Lapworth 1970; Vasil'ev 1990).

Powders of acrylic plastic ($d = 80 \div 300\,\mu\mathrm{m}, \rho_{22} = 1.2\,\mathrm{g/cm}^3$) and bronze ($d = 80 \div 130\,\mu\mathrm{m}, \rho_{22} = 8.6\,\mathrm{g/cm}^3$) were inserted into the channel by:

• an electromagnetic propelling device on the lower wall of the measurement section which threw the powder up to a required height;

• a vibrating grid on the upper lid of the measurement section creating a vertical flow of freely falling particles with a uniform concentration over the cross section. Interchangeable diaphragms in the grid allowed us to obtain a cloud with the geometry and particle concentration needed.

The dynamics of the SW/particles interaction were observed by fast-acting laser visualization methods in passing (multiframe shadow visualization method) and scattered (laser "knife" method) light. The exposure duration was 30 ns, the number of exposures and the intervals between them were defined by the laser stroboscope (Boiko et al. 1983). The frames were spatially separated in the high-speed camera by a rotating mirror prism. The accuracy of the time interval was $0.1\,\mu$s. The system of synchronization provided the required sequence of the starting of various elements of the shock tube and registering equipment. The generator originating a series of pulses was started by a piezoprobe located in the observation region. This provided an accuracy of the light pulse synchronization of as good as $1\,\mu$s with respect to the moment when the SW passes throught the region under study.

2.2 The effect of the particle concentration on the dynamics of their acceleration behind the shock wave

Consider some experimental data reflecting the dynamics of a cloud of particles behind the shock wave. Figures 2a,b show series of photos for two concentrations of the acrylic plastic particles: $m_2 < 0.2\%$ and $m_2 > 3\%$. As the cloud starts to move, it immediately becomes "blurred" both in longitudinal and transverse direction, hence, its mean concentration is reduced. One of the evident reasons for the increasing longitudinal size of the cloud is polydispersity. Small particles are accelerated faster than the large ones, which, alongside with the concentration decrease, leads to the particle separation by their size. The transverse expansion is connected to some extent with particles collisions but, as will be shown later, more essential are such effects as the transverse pressure gradient related to gas flow transformation.

Figure 3 shows the photos obtained for two kinds of particles (bronze, acrylic plastic) at $m_2 \leq 0.1\%$ and $m_2 > 1\%$. Figure 4 presents the trajectories of the front boundary of the cloud of bronze particles at $m_2 \sim 1\%$ and $m_2 < 0.1\%$. Similar plots $x(t)$ for acrylic plastic particles at $m_2 < 0.1\%$ and $m_2 \sim 3\%$ are given in Fig. 5. It is seen that the particles acceleration differs nearly by a factor of 2 when the concentration changes from $m_2 < 0.1\%$ to $m_2 \sim 1\%$.

In our opinion, the basic reason for such a pronounced effect of concentration on the dynamics of the particle acceleration in the cloud is caused by the change in the wave structure on the particles in supersonic flow. Indeed, the flow about the particles is supersonic at the initial stage of the particle acceleration behind the SW with a Mach number $M_0 > 2$. The photos presented in Fig. 6a,b indicate that at low concentration of the particles the leading shocks are formed near each one (a). When the concentration is increasing, the shock waves, interfering with each other, overlap and form a collective leading shock (b).

Before considering the particle dynamics in the cloud, one should examine in more detail the acceleration of a single particle in a supersonic flow behind the SW front. The drag coefficients were found in a special experimental series with spherical bronze particles of $d = 180 \pm 10\,\mu$m selected under the microscope. The range of variation of the relative Mach number $0.8 < M_{12} < 1.2$ corresponds to the change in the flow regime from supersonic to subsonic. A large amount of experiments carried out with particles of equal sizes showed that the spread in the absolute C_d values is no more than 10% and the mean C_d value and the behavior of $C_d = f(M)$ corre-

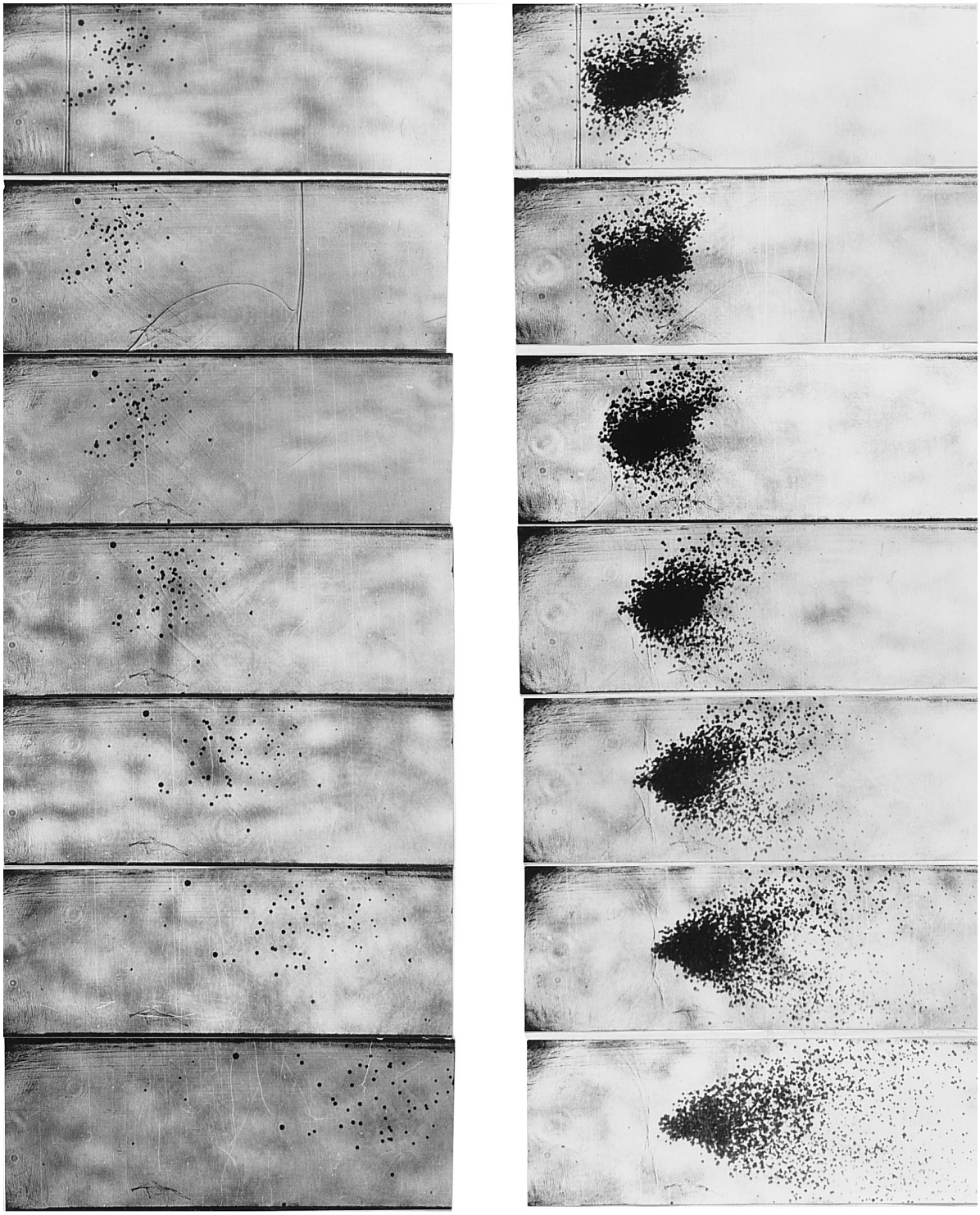

Fig. 2a,b. SW interaction with clouds of acrylic plastic for various concentrations of disperse phase: **a** $m_2 < 0.2\%$, **b** $m_2 > 3\%, M_0 = 4.5, p^0 = 0.01\,\text{MPa}, \Delta t = 20\,\mu\text{s}$

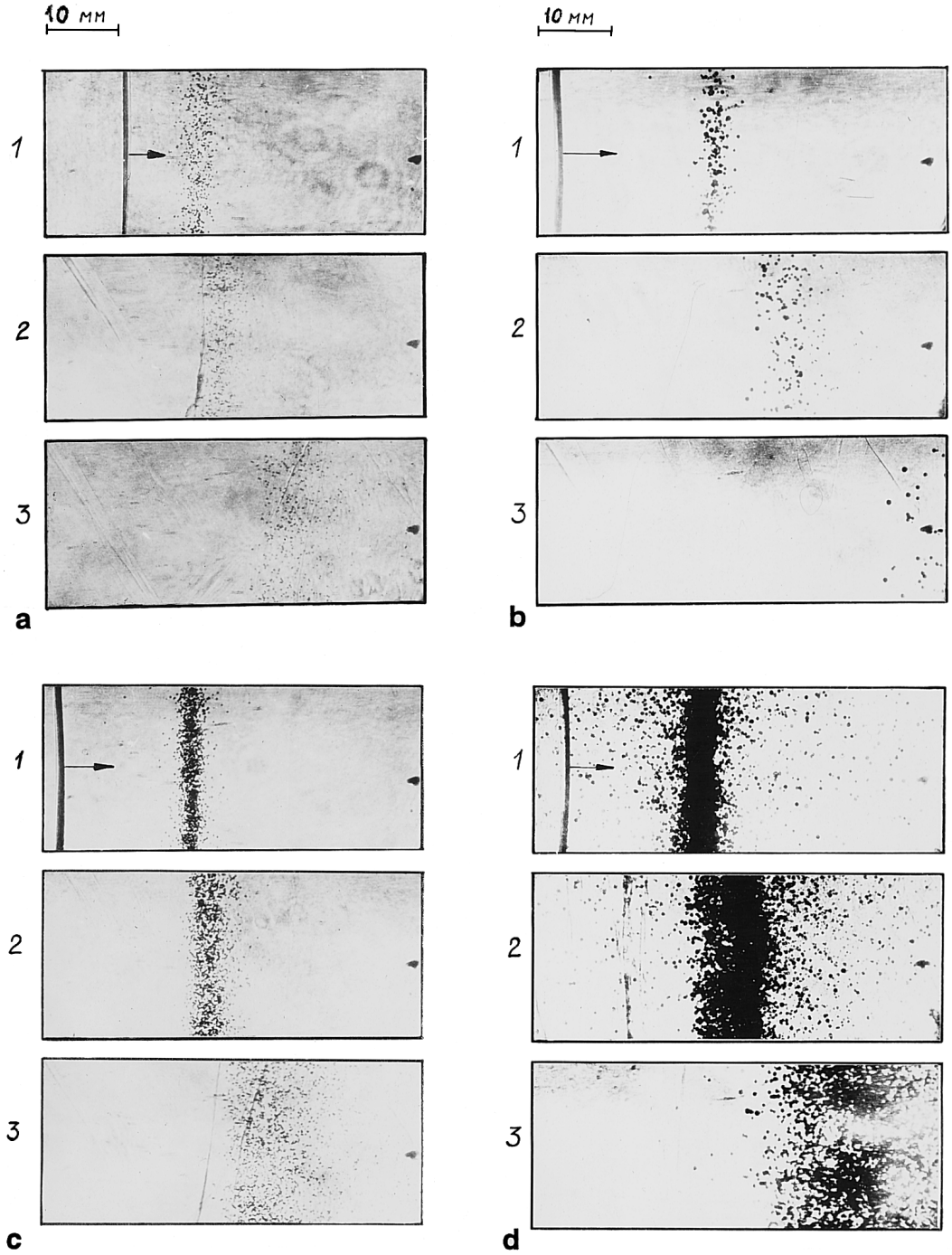

Fig. 3a–d. Two types of particles: bronze **a,b** and acrylic plastic **c,d** accelerated behind the SW: $m_2 \leq 0.1\%$ **a,b**; $m_2 > 1\%$ **c,d**. $M_0 = 2.8$, $p^0 = 0.1$ MPa, $\Delta t = 100\,\mu$s

sponds to the curve presented in Fig. 7. These data for a single spherical particle are well described by the formula

$$C_d(Re, M) = (0.38 + 24/Re + 4/Re^{0.5}) \times [1 + exp(-0.43/M_{12}^{4.67})] \quad (1)$$

This empirical formula will be used below in the numerical calculations.

The results obtained give grounds to argue that the observed effect is caused by the formation of a "collective" SW in front of the cloud. It results in the change of the flow about the particles from supersonic to subsonic, reduction of C_d and of dynamic pressure.

3 Mathematical simulation of the SW/cloud interaction

3.1 Continuum-discrete model of the gas/particles mixture

Consider a cloud of solid spherical particles impacted by the shock wave. The parameters of gas and particles resulting from

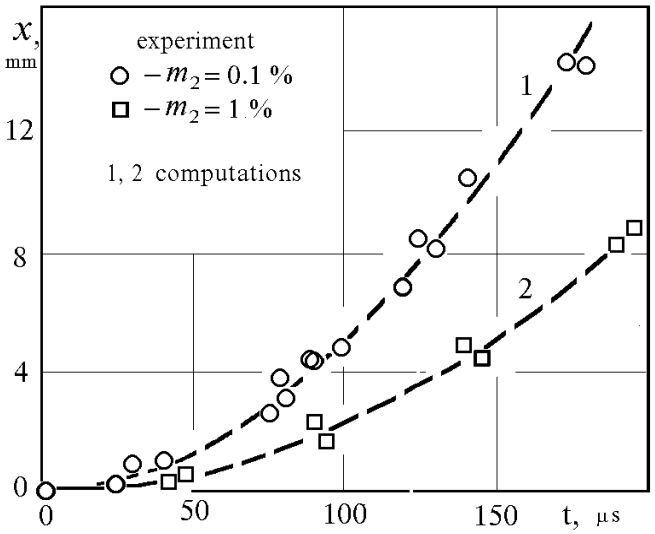

Fig. 4. Trajectories of bronze particles: $d = 80 \div 130\,\mu$m, $\rho_{22} = 8.6\,\mathrm{g/cm^3}$ at $m_2 < 1\%$ and $m_2 \sim 1\%$; computations for $d = 130\,\mu$m; $M_0 = 2.8$; $p^0 = 0.1$ MPa

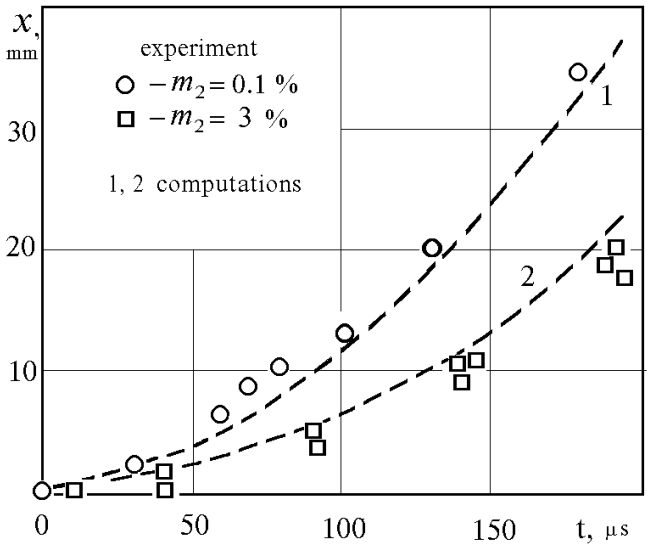

Fig. 5. Trajectories of acrylic plastic particles: $d = 80 \div 300\,\mu$m, $\rho_{22} = 1.2\,\mathrm{g/cm^3}$ for $m_2 < 1\%$ and $m_2 \sim 3\%$; computations for $d = 300\,\mu$m, $M_0 = 2.8$; $p^0 = 0.1$ MPa

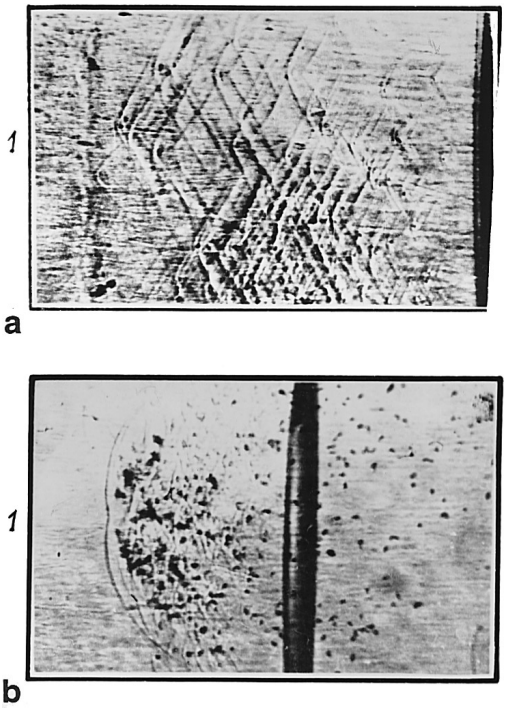

Fig. 6. Wave structure in a supersonic flow behind the SW with low $m_2 \leq 0.1\%$ **a** and high $m_2 > 1\%$ **b** concentration of particles in the cloud

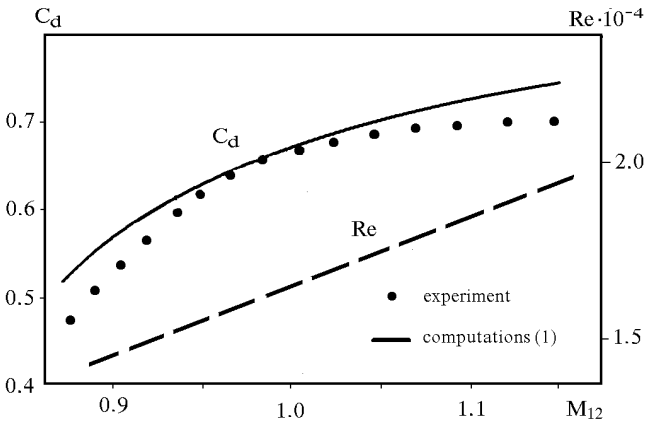

Fig. 7. Drag coefficient C_d of a particle as the function of the relative Mach number M_{12} of the flow

the SW/cloud interaction are to be found. The particle motion is simulated by a collisionless kinetic equation, the gas is modeled by the dusty gas equations. The particles are supposed to be dispersed in velocities and sizes. This model is described in detail in (Kiselev and Fomin 1986; Kiselev et al. 1992). It can be applied in the case when the particle trajectories intersect in the flow region and the particle collisions are scarce $\mathrm{Kn} \approx \mathrm{d}/(6\mathrm{m_2L}) \geq 1$, L is the distance covered by a particle in the cloud.

Let the x axis be directed along the velocity vector of the center of mass of the cloud of particles, and the y axis be perpendicular to it. For the plane case the collisionless kinetic equation has the following form in the system of the center of mass of the cloud of particles:

$$\frac{\partial f}{\partial t} + v_2\frac{\partial f}{\partial x} + w_2\frac{\partial f}{\partial y} + \frac{\partial}{\partial v_2}(a_x f) + \frac{\partial}{\partial w_2}(a_y f) + \frac{\partial}{\partial T_2}(qf) = 0, \tag{2}$$

where the velocity and acceleration of particles along the x axis are designated as v_2, a_x, and along the y axis - as w_2, a_y; T_2, q are the particles temperature and the specific heat flux to a particle. The velocities and accelerations in the system of the center of mass of the cloud of particles are related to

the velocities and accelerations in the laboratory coordinate system through the Galileo transforms:

$$v_2 = v_2^l - D, \quad a_x = a_x^l - \dot{D}, \quad w_2 = w_2^l, \quad a_y = a_y^l, \tag{3}$$

where the superscript l denotes parameters in the laboratory coordinate system. The velocity D and acceleration of the center of mass of the cloud are determined by the formulas

$$D = \frac{\int \rho_2 v_2^l f dV dV_0}{\int \rho_2 f dV dV_0}, \quad \dot{D} = \frac{dD}{dt}, \tag{4}$$

where $dV = dv_2 dw_2 dr_s dT_2$ is a volume element in the phase space, $dV_0 = dxdy$. The distribution function of particles f depends on time t, coordinates x, y, particle velocities v_2, w_2, particle radius r_s and temperature T_2. If f is known, then the concentration of particles n and the volume concentration of particles m_2 are found from the equations

$$n = \int f dV, \quad m_2 = \frac{4}{3}\pi \int r_s^3 f dV, \tag{5}$$

The quantity m_2 determines the fraction of unit volume occupied by particles. It is related to the volume concentration of gas by the equation

$$m_1 + m_2 = 1 \tag{6}$$

The components of the particle acceleration in the laboratory coordinate system are found from the formulas

$$a_x^l = \frac{v_1 - v_2}{\tau} - \frac{1}{\rho_{22}}\frac{\partial p}{\partial x}, \quad a_y^l = \frac{w_1 - w_2}{\tau} - \frac{1}{\rho_{22}}\frac{\partial p}{\partial y}, \tag{7}$$

where v_1, w_1 are the gas velocity components along the x and y axes, p is the gas pressure. The first component in (7) is conditioned by the difference in the velocity of gas and particles, and the second one appears due to the pressure gradient in the gas. The value of τ is determined by the character of the gas flow around the particle and is found by the formula

$$\frac{1}{\tau} = \frac{3}{4}\left(\frac{Re\mu}{\rho_{22} d^2}\right) C_d(Re, M_{12}), \tag{8}$$

where $C_d = C_d(Re, M_{12})$ is determined by formula (1), $Re = \rho_{12}|\mathbf{v}_1 - \mathbf{v}_2|d/\mu$ is the Reynolds number, $M_{12} = |\mathbf{v}_1 - \mathbf{v}_2|/c$ is the Mach number, $c = \sqrt{\gamma p/\rho_{11}}$ is the speed of sound, $d = 2r_s$ is the particle diameter, ρ_{22} is the density of the particle material, ρ_{11} is the true density of gas, μ is the viscosity of gas, $\gamma = c_p/c_v$, c_p, c_v are the specific heats of the gas at constant pressure and volume. The heat flux to the particle q is determined by the equations obtained by processing experimental data which have the form

$$q = 2\pi\lambda r_s Nu \frac{T_1 - T_2}{c_s m_s}, \quad Nu = 2 + 0.6 Re^{0.5} Pr^{0.33}, \tag{9}$$

where Nu is the Nusselt number, $Pr = c_p\mu/\lambda$ is the Prandtl number, λ is the heat conductivity of the gas, T_1 is the gas temperature, c_s is the specific heat of the particle, $m_s = (4/3)\pi r_s^3 \rho_{22}$ is the particle mass.

Let us write the equations of gas motion in vector form:

$$\frac{\partial \phi}{\partial t} + \frac{\partial F}{\partial x} + \frac{\partial G}{\partial y} + \Phi = 0, \tag{10}$$

where the vectors ϕ, F, G, Φ have the form

$$\phi = \begin{pmatrix} \rho_1 \\ \rho_1 v_1 \\ \rho_1 w_1 \\ \rho_1(E_1 + (v_1^2 + w_1^2)/2) \end{pmatrix},$$

$$F = \begin{pmatrix} \rho_1 v_1 \\ \rho_1 v_1^2 + p m_1 \\ \rho_1 v_1 w_1 \\ \rho_1 v_1 A_1 \end{pmatrix}, \tag{11}$$

$$G = \begin{pmatrix} \rho_1 w_1 \\ \rho_1 v_1 w_1 \\ \rho_1 w_1^2 + p m_1 \\ \rho_1 w_1 A_1 \end{pmatrix}, \quad \Phi = \begin{pmatrix} 0 \\ \Phi_1 \\ \Phi_2 \\ A_2 \end{pmatrix}.$$

The components of vector ϕ are $\rho_1 = \rho_{11} m_1$, the mean density of the gas; $\rho_1 v_1, \rho_1 w_1$, the momenta densities of the gas along the x and y axes ($v_1 = v_1^l - D, w_1 = w_1^l$); $E_1 = c_v T_1$, the specific energy of the gas; $\rho_1(E_1 + (v_1^2 + w_1^2)/2)$, the mean energy density of the gas. The components of vectors F and G are the fluxes of the above quantities along the x and y axes, and $A_1 = H_1 + (v_1^2 + w_1^2)/2$ where $H_1 = E_1 + p m_1/\rho_1$ is the specific enthalpy of the gas. The components of vector Φ designated as Φ_1 and Φ_2 describe the force affecting the gas from the particles along the x and y axes:

$$\Phi_1 = -p\frac{\partial m_1}{\partial x} + \int m_s \frac{(v_1 - v_2)}{\tau} f dV,$$
$$\Phi_2 = -p\frac{\partial m_1}{\partial y} + \int m_s \frac{(w_1 - w_2)}{\tau} f dV. \tag{12}$$

The fourth component A_2 determines the energy exchange between the gas and particles:

$$A_2 = v_1\Phi_1 + w_1\Phi_2 + p\left(\frac{\partial m_1}{\partial t} + v_1\frac{\partial m_1}{\partial x} + w_1\frac{\partial m_1}{\partial y}\right) - \rho_1\Phi_3, \tag{13}$$

where

$$\Phi_3 = \frac{1}{\rho_1}\int m_s\left(\frac{(v_1 - v_2)^2}{\tau} + \frac{(w_1 - w_2)^2}{\tau} - c_s q\right) f dV. \tag{14}$$

The equations of state for the perfect gas have the form

$$p = (\gamma - 1)\rho_{11} E_1. \tag{15}$$

The condition of incompressibility is assumed valid for the particles: $\rho_{22} = \text{const}$.

The system of Eqs. (2–15) is used below for computing subsonic and supersonic flows of gas and particles. This model gives no way of computing the shock on each particle but the Mach SW is taken into account in the function $C_d(M_{12})$. This provides a possibility to correctly describe the averaged supersonic motion of the cloud of particles in the gas.

3.2 Computational algorithm

The system of Eqs. (2–15) is numerically solved with the following algorithm. An Euler rectangular grid is built on the (x, y) plane with the steps in x, y directions equal to $2h_x, 2h_y$, respectively. Equations for gas are written according to the explicit finite-difference scheme of third order accuracy (Rusanov 1968; Gridnev et al. 1984).

The collisionless kinetic equation is solved in Lagrangian variables. Take an individual volume in the phase space of particles $\theta(t)$. The condition of the constant total number of particles N in the individual volume is

$$N = \int_{\theta(t)} f dV_0 dV = const, \tag{16}$$

where $\theta(t)$ is formed by the same particles whose trajectories are found from

$$\begin{aligned} &\frac{dx}{dt} = v_2, \quad \frac{dy}{dt} = w_2, \quad \frac{dv_2}{dt} = a_x, \\ &\frac{dw_2}{dt} = a_y, \quad \frac{dT_2}{dt} = q, \quad \frac{dr_s}{dt} = 0. \end{aligned} \tag{17}$$

Equations (17) coincide with the characteristics of the kinetic equation (Eq. (2)), the last equation reflects the absence of particle splitting and coagulation. Differentiating (16) with respect to time, with account of the Ostrogradskii-Gauss theorem and system (17) one can easily obtain the collisionless kinetic Eq. (2). The individual volume $\theta(t)$ coincides with the volume of a moving cell, hence, the number of particles in the i-th cell is constant. The region occupied by particles is split at the moment $t = 0$ into rectangular Lagrangian cells of the size $2h_x, 2h_y$ so that inside every i-th cell all particles have equal velocity v_{2i}^0, w_{2i}^0, temperature T_{2i}^0 and radius r_i. Therefore, the distribution function in the i-th cell at $t = 0$ is

$$\begin{aligned} &f_i = \frac{N_i}{V_i^0}\delta(v_2 - v_{2i}^0)\delta(w_2 - w_{2i}^0)\delta(r_s - r_i)\delta(T_2 - T_{2i}^0), \\ &V_i^0 = 4h_x h_y, \end{aligned}$$

where V_i^0 is the volume of the cell, N_i is the number of particles in the i-th cell and δ is the delta function. The number of particles in the i-th cell is constant, therefore the distribution function in the i-th cell at the moment n is determined by

$$\begin{aligned} &f_i^n = \frac{N_i}{V_i^n}\delta(v_2 - v_{2i}^n)\delta(w_2 - w_{2i}^n) \\ &\qquad \times \delta(r_s - r_i)\delta(T_2 - T_{2i}^n), \\ &V_i^n = 4h_x h_y. \end{aligned} \tag{18}$$

The particle parameters at the instant t^n are determined from the difference equations which provide the first-order approximation in time of the system of ordinary differential Eqs. (17). For the particle velocities and temperature we have

$$\begin{aligned} &v_{2i}^n = v_{2i}^{n-1} + \tau a_{xi}^{n-1}, \qquad w_{2i}^n = w_{2i}^{n-1} + \tau a_{yi}^{n-1}, \\ &T_{2i}^n = T_{2i}^{n-1} + \tau q_i^n, \end{aligned} \tag{19a}$$

where $\tau = t^n - t^{n-1}$ is the time step. Having differentiated the first two equations in (17) with respect to time and taking into account the third and fourth equations in (17), we obtain the corresponding difference equations

$$\begin{aligned} &x_{2i}^n = x_{2i}^{n-1} + \tau v_{2i}^{n-1} + \tau^2 a_{xi}^{n-1}/2, \\ &y_{2i}^n = y_{2i}^{n-1} + \tau w_{2i}^{n-1} + \tau^2 a_{yi}^{n-1}/2. \end{aligned} \tag{19b}$$

As it follows from (19), the Lagrangian cells move with respect to the Euler grid with the velocities v_{2i}^n, w_{2i}^n. The distribution function f_j^n in the j - Euler cell is

$$\begin{aligned} f_j^n = \sum_i^m &\frac{\delta_i^n N_i}{V_i^n}\delta(v_2 - v_{2i}^n)\delta(w_2 - w_{2i}^n) \\ &\times \delta(r_s - r_i)\delta(T_2 - T_{2i}^n), \end{aligned} \tag{20}$$

where δ_i^n is the volume fraction occupied by the i-th cell in the j-th Euler cell. The summation in (20) is performed over m cells crossing the j-th Euler cell. Equations (20) are used to find the mean value of $\langle \mathcal{Q} \rangle$:

$$\langle \mathcal{Q} \rangle = \frac{1}{n} \int \mathcal{Q} f dV. \tag{21}$$

Substituting (20) into (21) yields $\langle \mathcal{Q} \rangle_j^n$ in the j-th Euler cell

$$\langle \mathcal{Q} \rangle = \frac{\sum_i^m \mathcal{Q}_i^n \delta_i^n N_i / V_i^n}{\sum_i^m \delta_i^n N_i / V_i^n}. \tag{22}$$

Formula (22) allows one to find the mean parameters of the particles in a random Euler cell. The gas parameters in the cell were found by the linear interpolation method. Methodically this technique of solving numerically the kinetic equation is close to the particles method in rarefied plasma dynamics (Berezin and Fedoruk 1993). However, there are some essential differences. In this paper the dusty gas equations are solved together with the kinetic equation while in (Berezin and Fedoruk 1993) Maxwell equations are solved. In the steady state a similar method for computing gas/particles flows was suggested by Crow (1982).

3.3 One-dimensional calculation of SW/cloud interaction

Let us compute the two-phase flow and study the dynamics of the leading edge of a cloud of spherical particles behind the SW. A homogeneous cloud covers the cross section of a flat channel (see Fig. 8).

In the region Ω_1 (without particles) the gas parameters are computed from the Euler equations (perfect gas) with third-order accuracy. In the region Ω_2 the system of Eqs. (2–15) was solved using the numerical technique described in 3.2, under the assumption that $dD/dt = 0$ (laboratory frame of reference).

Ahead of the shock wave $x > x^+$ the gas is at rest, therefore,

$$\rho_{11} = \rho_{11}^0, \qquad p = p^0, \qquad v_1 = w_1 = 0. \tag{23}$$

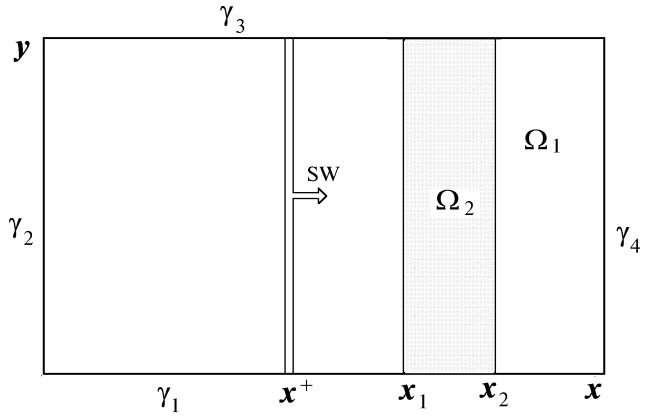

Fig. 8. Computational domain (one-dimensional case); Ω_1 is the region occupied by the gas; Ω_2 is the gas/particles mixture; x^+ is the SW front coordinate; x_1 is the front boundary of the cloud; x_2 is the rear boundary of the cloud; $\gamma_1 \div \gamma_4$ are the computational domain boundaries

The gas parameters behind the shock wave $x < x^+$ are found from the Hugoniot condition

$$\rho_{11} = \frac{\rho_{11}^0 M_0^2}{1 - h + hM_0^2}, \quad p = p^0\big((1+h)M_0^2 - h\big),$$
$$v_1 = (1-h)c_0(M_0 - 1/M_0), \qquad w_1 = 0, \tag{24}$$

where $h = (\gamma - 1)/(\gamma + 1)$, $M_0 = D_0/c_0$ is the shock wave Mach number. It is assumed that the particles in the cloud are at rest and have the same radius $d_s/2$ and temperature T_0, thus in Ω_2

$$f^0 = \frac{6m_2^0}{\pi d_s^3}\delta(r_s - d_s/2)\delta(w_2)\delta(v_2)\delta(T_2 - T_2^0). \tag{25}$$

The boundary conditions for γ_1, γ_3 were $w_1 = 0$, for γ_2, γ_4 – $\partial\phi/\partial x = 0$ (see Fig. 8). For γ_1, γ_3 the mirror reflection of particles was assumed, for γ_2, γ_4 the no-slip condition was taken. The parameter values of gas and particles for the computations were selected the same as in the experiments described in 2.2. The computed trajectories of the left boundary $x(t)$ of a cloud of monodisperse particles of acrylic plastic ($d_s = 300\,\mu$m) are presented in Fig. 5 (1, 2). The computed and experimental results are in a good agreement.

Figures 9, 10 show the plots of pressure p and the Mach number $M_1(x)$ for a dense cloud. A reflected (collective) SW is seen to form in front of the cloud. Inside the cloud an expansion wave is formed where the gas accelerates and the flow becomes supersonic near the right boundary of the cloud. The amplitude of the travelling SW decreases as compared with the incident SW because some part of the gas energy is spent for the cloud acceleration.

Figure 11 gives the dependence of $M_1(x)$ for the SW interaction with the rarefied cloud of acrylic plastic particles with a small volume concentration of the particles. The flow in the cloud is supersonic and no reflected collective SW appears. The appearance of small disturbances in front of the left boundary is related to the scheme viscosity.

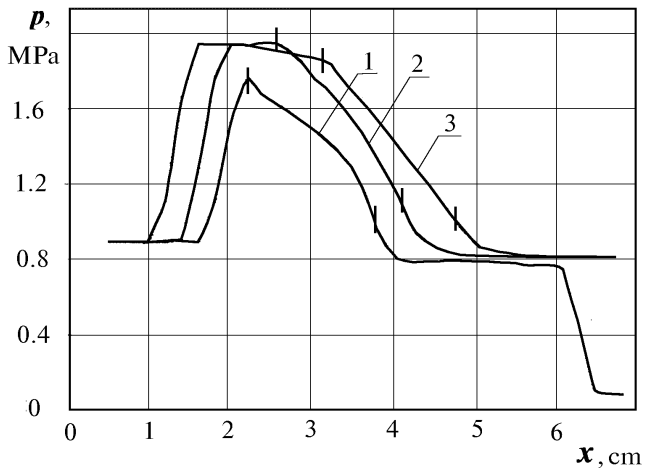

Fig. 9. Pressure profiles $p(x)$ in the cloud of acrylic plastic particles in the time moments $50, 100, 150\,\mu$s $(1, 2, 3)$, $m_2 = 3 \cdot 10^{-2}$. The vertical lines denote the cloud boundaries (the same in Figs. 10, 11)

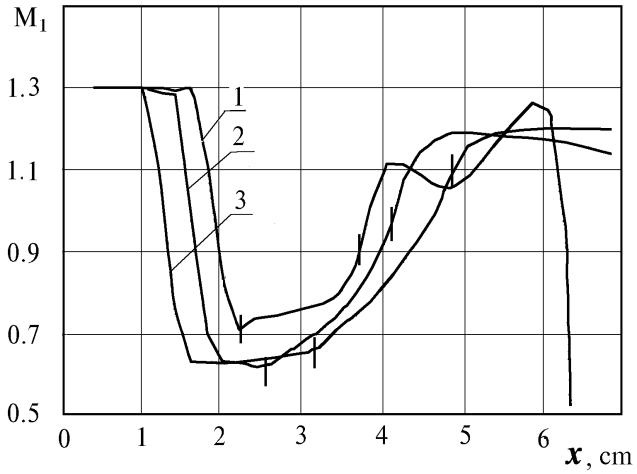

Fig. 10. The flow Mach number profiles $M_1(x)$ under the conditions shown in Fig. 9

The plot $x(t)$ for acceleration of the bronze particles cloud is shown in Fig. 4 (1, 2).

3.4 Two-dimensional computation of SW/cloud interaction

Let a SW be incident to a cloud of spherical particles of acrylic plastic in the region Ω_2 bounded in x and y directions (see Fig. 12). Consider a $2D$ case: the motion of the gas and particles is described by Eqs. (2). At the time moment $t = 0$ the cloud has a rectangular shape. The particles are monodisperse $d = 100\,\mu$m, $\rho_{22} = 1.2\,\mathrm{g/cm^3}$, $T_2^0 = 300\,\mathrm{K}$, $v_2 = w_2 = 0$, $m_2^0 = 10^{-2}$. The SW Mach number is $M_0 = 3$ and the gas parameters in front of the shock wave are found from the Hugoniot conditions at $\rho_{11}^0 = 1.3\,\mathrm{kg/m^3}$, $T_1^0 = 300\,\mathrm{K}$. At the boundary γ_1, we assumed $w_1 = 0$, at γ_2, γ_4 – $\partial\phi/\partial x = 0$, at γ_3 – $\partial\phi/\partial y = 0$. The mirror reflection was assumed for the particles on γ_1 and no-slip condition on $\gamma_2, \gamma_3, \gamma_4$.

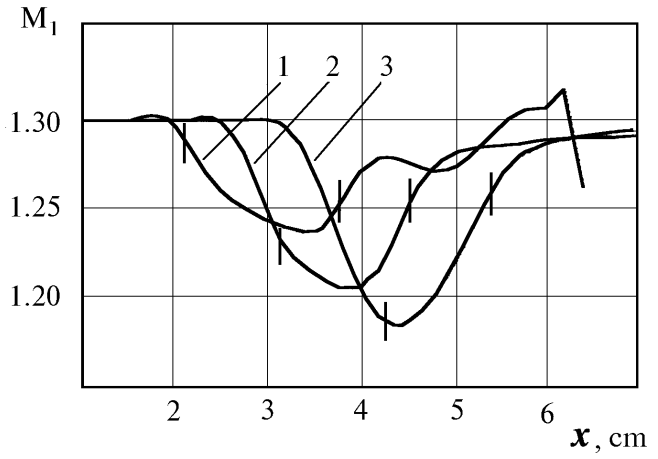

Fig. 11. The flow Mach number profiles $M_1(x)$ in the cloud of acrylic plastic particles at $m_2 = 10^{-3}$

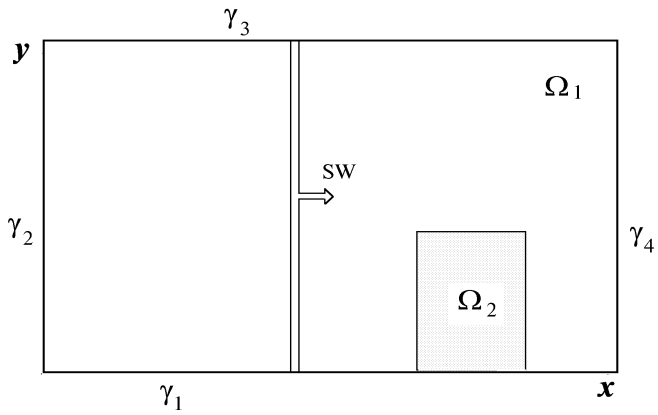

Fig. 12. Computational domain (two-dimensional case). Notations are the same as in Fig. 8

Figures 13a,b show the isobars $p(x, y)$ for the time moments 80 and 160 μs. A reflected shock wave is seen to be formed in front of the cloud. Inside the cloud a constant negative pressure gradient (expansion wave) develops. The gas/particle interaction force decreases in time $f_{12} \sim C_d(v_1 - v_2)$ as a result of the particle cloud acceleration. Therefore, an expansion wave starts to propagate upstream from the cloud, which attenuates the reflected SW. The pressure behind the SW is determined from the discontinuity appearing at the moment the expansion wave reaches the reflected SW front. This process is a nonsteady one. The time of the expansion wave coming to a certain point of the SW depends on its location, namely, it increases with the transverse coordinate growth. Thus, the pressure behind the SW and, hence, the SW propagation velocity on the periphery is greater than near the axis (semispace boundary). The reflected SW front starts to straighten, while the shock wave itself separates from the cloud, which is well seen in Fig. 13.

Figure 14 presents the isolines of the volume particle concentration $m_2(x, y)$. Since the gas velocity is not uniform behind the SW, the cloud is seen to expand upwards and to extend

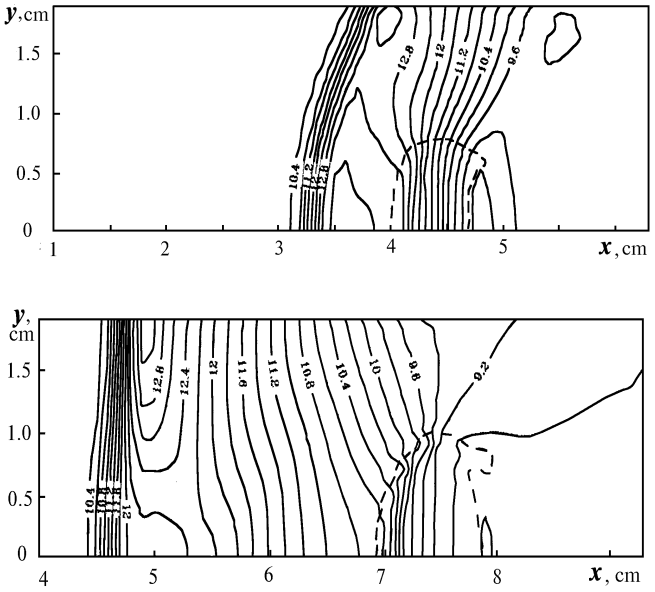

Fig. 13. Isobars $p(x, y)$ (atm) for the time moment 80 μs **a** and 160 μs **b**. The dashed line is the cloud boundary (laboratory frame of reference)

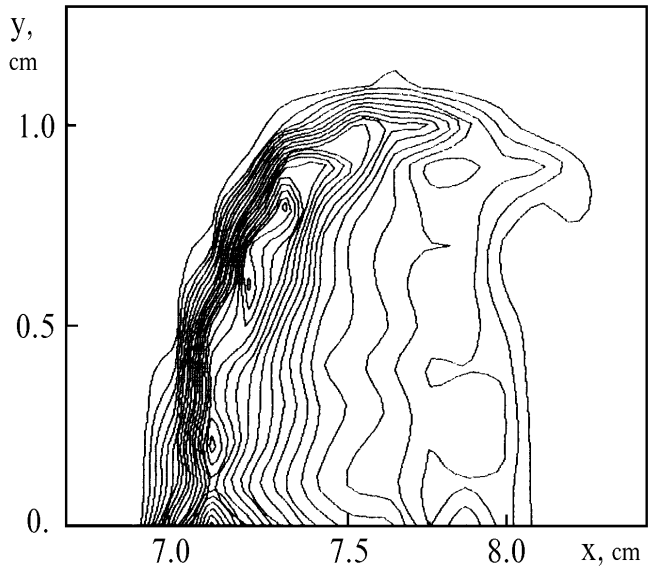

Fig. 14. Isolines of the volume concentration $m_2(x, y)$ with the step $\Delta m_2 = \cdot 10^{-3}$ for the time moment 160 μs (laboratory frame of reference).

downstream. The region of higher concentration is formed at the windward side of the cloud. Figure 15 shows the velocity field of the particles in the system of the cloud center of mass. The particle trajectories are seen to gather near the front cloud boundary, i.e. the edge caustic shown in Fig. 16 develop.

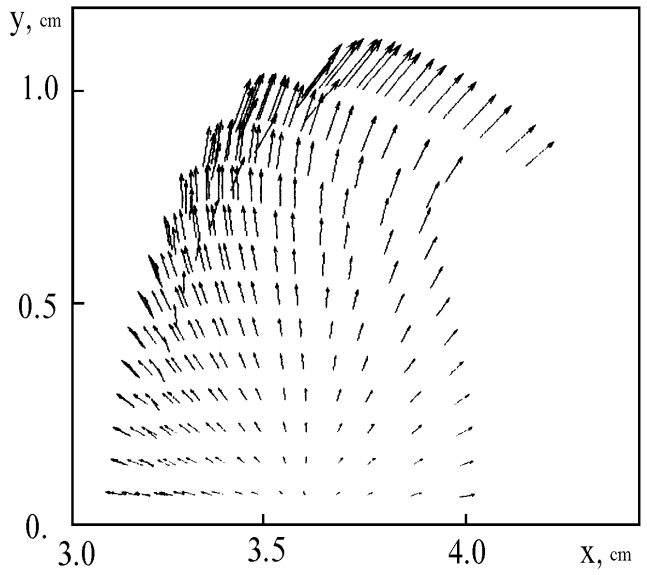

Fig. 15. Velocity field of acrylic plastic particles in the center of mass system

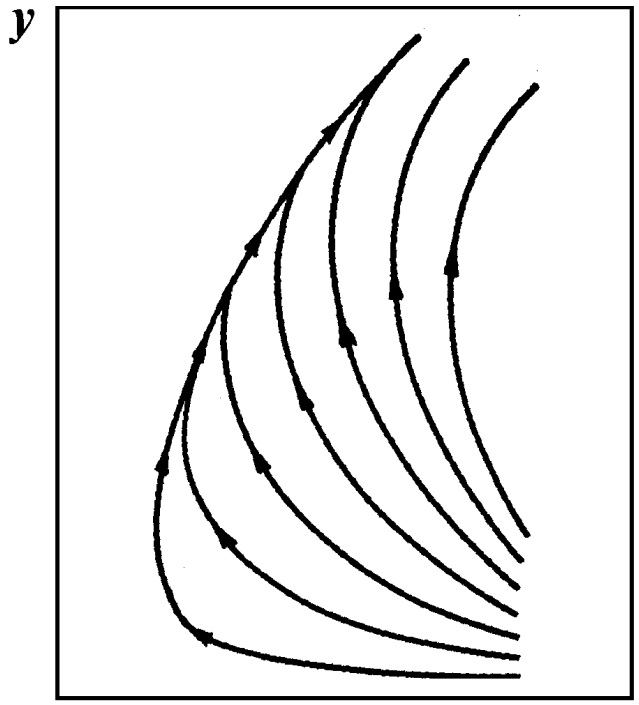

Fig. 16. Trajectories of particles

4 Discussion

Two mechanisms of a "collective" SW formation in front of a cloud of particles are known at present. According to Blagosklonov et al. (1979) a collective bow shock wave is formed when transonic regions merge behind the shocks on separate particles. In this case the condition of its appearance is determined by the relation $l/d \le l^*/d$ where l^* is the characteristic size of the transonic region. The ratio l^*/d grows with M_1 decreasing but does not exceed $l^*/d \sim 5$ according to the estimates of Blagosklonov et al. (1979) because the shock intensity is reduced. Therefore, the formation of the "collective" bow SW should be expected if $l^*/d \le 5$, the volume concentration being $m_2 \sim (l^*/d)^{-3} > 0.01$.

If $m_2 \le 0.01$ another mechanism of the "collective" bow shock wave is established, which allows one to consider it as a reflected SW. The supersonic flow penetrates into the cloud of the gas/particles mixture to some depth l. As a result of gradual gas deceleration on the section l a compression wave appears which transforms in time into a reflected SW. Then the time of the reflected SW formation t^* must be of the order of the gas deceleration time τ_v. Let us evaluate τ_v from the gas motion equation

$$\frac{dv_1}{dt} = -\frac{1}{\rho_{11}}\frac{\partial p}{\partial x} - \frac{3}{4}C_d\frac{m_2}{m_1}|v_1 - v_2|(v_1 - v_2)/d \qquad (26)$$

At the stage of the collective SW formation the velocity v_2 of the particles is essentially smaller than the gas velocity $v_1 (v_2 \ll v_1)$, hence, the second term in the right-hand part may be presented as $-v_1/\tau_v$, where

$$\tau_v = \frac{4}{3}\frac{m_1}{C_d m_2}\frac{d}{v_1}.$$

Herefrom at $v_1 \approx 7{\cdot}10^2$ m/s, $d_s = 300\,\mu$m, $m_2 = 3{\cdot}10^{-2}$, $C_d \sim 1-0.5$, we have $\tau_v \sim 20-40\,\mu$s, which is close to $t^* \sim 50\,\mu$s according to Figs. 3d, 9, 10.

The analysis of the gas flow makes it possible to understand the reason for higher acceleration of the rarefied cloud of particles. In this case for the acrylic plastic particles the gas velocity in the rarefied cloud ($m_2^0 \approx 10^{-3}$) is approximately twice as high as in a dense cloud ($m_2^0 \approx 10^{-2}$) (see Figs. 10, 11). Another factor affecting the particle acceleration is the dependence $C_d = C_d(M_{12})$. As was noted above (section 2.2), this is connected with the change of the flow about the particles from supersonic to subsonic in dense clouds.

The force acting on a particle is $f_{12} \sim C_d\rho_{11}(v_1 - v_2)^2/d$. The particle velocity $v_1 \gg v_2$ may be neglected at the initial stage of acceleration for $t \le 100\,\mu$s, therefore, $f_{12} \sim C_d\rho_{11}v_1^2/d$. The value of $j = \rho_{11}v_1$ is approximately the same for dense and rarefied clouds. Thus, the difference in the f_{12} dependence on the dynamic pressure for dense and rarefied clouds is reduced to $f_{12} \sim C_d v_1$.

The computations showed that at the time moment $t \approx 50\,\mu$s $C_d \approx 0.44$ at $m_2^0 = 3 \cdot 10^{-2}$ and $C_d = 0.72$ at $m_2^0 = 10^{-3}$, hence, neglecting in the first approximation the dependence j on m_2^0 we get the estimate

$$\frac{x_1^d}{x_1^r} \approx \frac{f_{12}^d}{f_{12}^r} \approx \frac{C_d^d}{C_d^r}\frac{v_1^d}{v_1^r} \approx 0.3$$

where the superscript "d" means the values for $m_2^0 = 3 \cdot 10^{-2}$ and "r" denotes the values for $m_2^0 = 10^{-3}$. This estimate holds also for later time when v_2 cannot be neglected. The analysis of the flow of gas and acrylic plastic particles taken in the middle of the cloud at $t = 150\,\mu$s yields

$$\frac{f_{12}^d}{f_{12}^r} \approx \frac{C_d^d(v_1 - v_2)^d}{C_d^r(v_1 - v_2)^r} \approx 0.42.$$

Note that for the acceleration of the bronze particles the difference in f_{12}^d and f_{12}^r is mostly related to the $C_d(M_{12})$ dependence. For the moment t = 150μs $(v_1 - v_2)^d/(v_1 - v_2)^r \sim 0.75, C_d^d/C_d^r \sim 0.55, f_{12}^d/f_{12}^r \sim 0.4$.

5 Conclusion

The results of an experimental and theoretical study of the shock wave interaction with a cloud of solid particles are presented in the paper. It is shown experimentally that a reflected shock wave is formed ahead of the cloud of particles at volume concentration of particles about 1-3%. Numerical simulation of the problem carried out on a PC allowed one to reveal the formation mechanism of the reflected shock wave. A compression wave arises in the cloud due to deceleration of gas by the particles. Because of nonlinear effects the compression wave is transformed into a shock wave which moves towards the gas flow. In the course of time the shock wave leaves the cloud, and a rarefaction wave is formed in the cloud of particles, where the gas flow is accelerated. The final state of the gas behind the cloud of particles is determined by irreversible losses of the gas flow in the shock wave and in the cloud of particles due to friction and heat exchange with the particles. The described mechanism of formation of a shock wave reflected on a cloud of particles is universal and valid for volume concentrations of particles of the order of several percent.

References

Bailey AB, Hiatt J (1972) Sphere Drag Coefficient for a Broad Range of Mach and Reynolds Numbers. AIAA J 10:1436–1440

Bailey AB, Starr RF (1976) Sphere Drag at Transonic Speeds and High Reynolds Numbers. AIAA J 14:1631–1632

Berezin YuA, Fedoruk MP (1993) Simulation of Unsteady Plasma Processes. Nauka, Novosibirsk (in Russian)

Blagosklonov VI, Kuznetsov VM, Minailos AN et al. (1979) On Interference of Hypersonic Nonuniform Flows. J Appl Mech & Tech Phys (Translated from Russian) 5:59–67

Boiko VM, Fedorov AV, Fomin VM, Papyrin AN, Soloukhin RI (1983) Ignition of Small Particles Behind Shock Waves. In: Bowen TR, Manson N, Oppenheim AK, Soloukhin RI (eds) Shock Waves, Explosions and Detonations. Progress in Astronautics and Aeronautics, vol 87, AIAA Inc NY, pp 71–83

Carlson DJ, Hoglund RF (1964) Particle Drag and Heat Transfer in Rocket Nozzles. AIAA J 2:1980–1984

Crow (1982) Numerical Models for Dilute Gas-Particle Flows. Washington State Univ Review

Gorbis ZP (1964) Heat Exchange in Disperse Flows. Energiya, Moscow (in Russian)

Gridnev NP, Katsnel'son SS, Fomichev VP (1984) Nonuniform MHD-flows with E-layer. Nauka, Novosibirsk (in Russian)

Henderson CB (1976) Drag Coefficient of Spheres in Continuum and Rarefied Flows. AIAA J 14:707–708

Ivandaev AI, Kutushev AG, Nigmatulin RI (1981) Gas Dynamics of Multiphase Media. Shock and Detonation Waves in Gas Mixtures. In: Fluid and Gas Mechanics. Vol.16, Scientific and Engineering Review, VINITI AN SSSR, Moscow, pp 209-287 (in Russian)

Kiselev SP, Fomin VM (1986) Continual-Discrete Model for Gas/Solid Particles Mixture at Small Volume Concentration of Particles. J Appl Mech & Tech Phys (Translated from Russian) 2:93–101

Kiselev SP, Ruev GA, Trunev AP et al. (1992) Shock Wave Processes in Two-Component and Two-Phase Media. Nauka, Novosibirsk (in Russian)

Kiselev VP, Kiselev SP, Fomin VM (1994) Interaction of a Shock Wave with a Cloud of Particles of Finite Dimensions. J Appl Mech & Tech Phys (Translated from Russian) 2:26–37

Lapworth KC (1970) Normal Shock Wave Tables for Air, ... and Oxygen. ARS Current Papers

Rudinger G (1970) Effective Drag Coefficient for Gas-Particle Flow in Shock Tubes. ASME Trans 920:165–172

Rusanov VV (1968) Third-Order Difference Scheme for a Through Calculation of Discontinuum Solutions. Dokl AN SSSR 180:1303–1305 (in Russian)

Selberg BP, Nicholls JA (1968) Drag Coefficient of Small Spherical Particles. AIAA J 6:401–408

Soo SL (1971) Fluid Dynamics of Multiphase Systems. Mir, Moscow

Vasil'ev AA (1990) Shock Waves Parameters in Gases: Methodical Notes Part 1. NGU, Novosibirsk (in Russian)

Yanenko NN, Soloukhin RI, Papyrin AN, Fomin VM (1980) Supersonic Two-Phase Flows with Velocity Nonequilibrium of Particles. Nauka, Novosibirsk (in Russian)